Magnetic Resonance Imaging and Bioelectrical Impedance Analysis to Assess Visceral and Abdominal Adipose Tissue

Oliver Chaudry (iD) [1,2], Alexandra Grimm[1], Andreas Friedberger[1], Wolfgang Kemmler[1], Michael Uder[3], Franz Jakob[4], Harald H. Quick[1,5,6], Simon von Stengel[1], and Klaus Engelke[1,2]

Objective: This study aimed to compare a state-of-the-art bioelectrical impedance analysis (BIA) device with two-point Dixon magnetic resonance imaging (MRI) for the quantification of visceral adipose tissue (VAT) as a health-related risk factor.

Methods: A total of 63 male participants were measured using a 3-T MRI scanner and a segmental, multifrequency BIA device. MRI generated fat fraction (FF) maps, in which VAT volume, total abdominal adipose tissue volume, and FF of visceral and total abdominal compartments were quantified. BIA estimated body fat mass and VAT area.

Results: Coefficients of determination between abdominal ($r^2 = 0.75$) and visceral compartments ($r^2 = 0.78$) were similar for both groups, but slopes differed by a factor of two. The ratio of visceral to total abdominal FF was increased in older men compared with younger men. This difference was not detected with BIA. MRI and BIA measurements of the total abdominal volume correlated moderately ($r^2 = 0.31\text{-}0.56$), and visceral measurements correlated poorly ($r^2 = 0.13\text{-}0.44$).

Conclusions: Visceral BIA measurements agreed better with MRI measurements of the total abdomen than of the visceral compartment, indicating that BIA visceral fat area assessment cannot differentiate adipose tissue between visceral and abdominal compartments in young and older participants.

Study Importance

What is already known?

► Visceral adipose tissue, which is relevant for several pathologies, is commonly assessed by magnetic resonance imaging (MRI) using different scanning protocols. Biolelectrical impedence analysis (BIA) is often used as a cost-effective and widely available alternative to MRI when quantifying total adipose tissue.

What does this study add?

► This study compares BIA with Dixon fat fraction map results and volumetric fat measurements with direct fat fraction results.

Introduction

Obesity and sarcopenia are severe consequences of the sedentary lifestyle in industrialized nations. Both conditions are associated with increased morbidity, mortality, and socioeconomic costs (1-7). Initially, adipose tissue was regarded as inert tissue, only of importance to store excess energy of the body. However, newer research has shown that adipose tissue is also a source of hormones and proinflammatory cytokines (2) and that it affects the cardiovascular, musculoskeletal, metabolic, and central nervous systems (4). The two major types of adipose tissue are subcutaneous adipose tissue (SAT), located underneath the skin, and visceral adipose tissue (VAT), located inside the abdominopelvic cavity among the visceral organs (8). SAT and VAT are both associated with classic obesity-related pathologies, such as the metabolic syndrome (9-11), but effects of SAT and VAT on health-related risk factors differ (12). Therefore, it is important to assess SAT and VAT separately.

Three-dimensional imaging methods, such as magnetic resonance imaging (MRI) and computed tomography, provide a map of the spatial distribution of SAT and VAT (13) in the human body. In addition, the water-fat composition can be estimated by the computed tomography density or by quantitative MRI such as Dixon sequences (14,15). Using modified gradient echo or spin echo pulse sequences, Dixon techniques exploit differences in resonance frequencies (chemical shift)

to decompose fat and water components of the proton signal into two separate image maps (16). The resulting water-only and fat-only images can be combined to parametric fat fraction (FF) or water fraction maps (17,18). The gray values of the FF map directly code the amount of fat as a percentage. A gray value of 1,000 corresponds to a FF of 100%, and a gray value of 100 corresponds to a FF of 10%. FF cannot be measured in standard clinical T1-weighted images.

If the determination of the spatial distribution of FF across the body is less relevant, bioelectrical impedance analysis (BIA) is a fast and cost-effective method to estimate fat-free tissue and fat mass from impedance measurements within a given part of the body. Because of technological advances in the past decade, extracellular and intracellular water can be estimated by using multifrequency BIA, and separate arm, leg, and trunk measurements can be obtained with segmental BIA (19).

The purpose of this cross-sectional study is to compare VAT as determined with segmental, multifrequency BIA with the measurements of VAT volume and direct FF values from two-point Dixon MRI, which is used as the gold standard.

Methods

Subject population

Two groups (group 1 [G1] and group 2 [G2]) with a total of 63 participants were recruited for the study (Table 1). G1 consisted of 25 young healthy participants (mean age 28 (SD 4) years; range: 21-36 years). G2 consisted of 38 older participants (mean age 76 (SD 5) years; range: 70-86 years), a subset of participants of the epidemiological sarcopenic obesity study (20). The study complied with the Declaration of Helsinki's "Ethical Principles for Medical Research Involving Human Subjects" and it was approved by the local university ethics committee of Friedrich-Alexander University Erlangen-Nürnberg (application No. 67_15b and 187_16B). After detailed information, all study participants gave their written informed consent. Consent for publication was given from all participants, and data were anonymized.
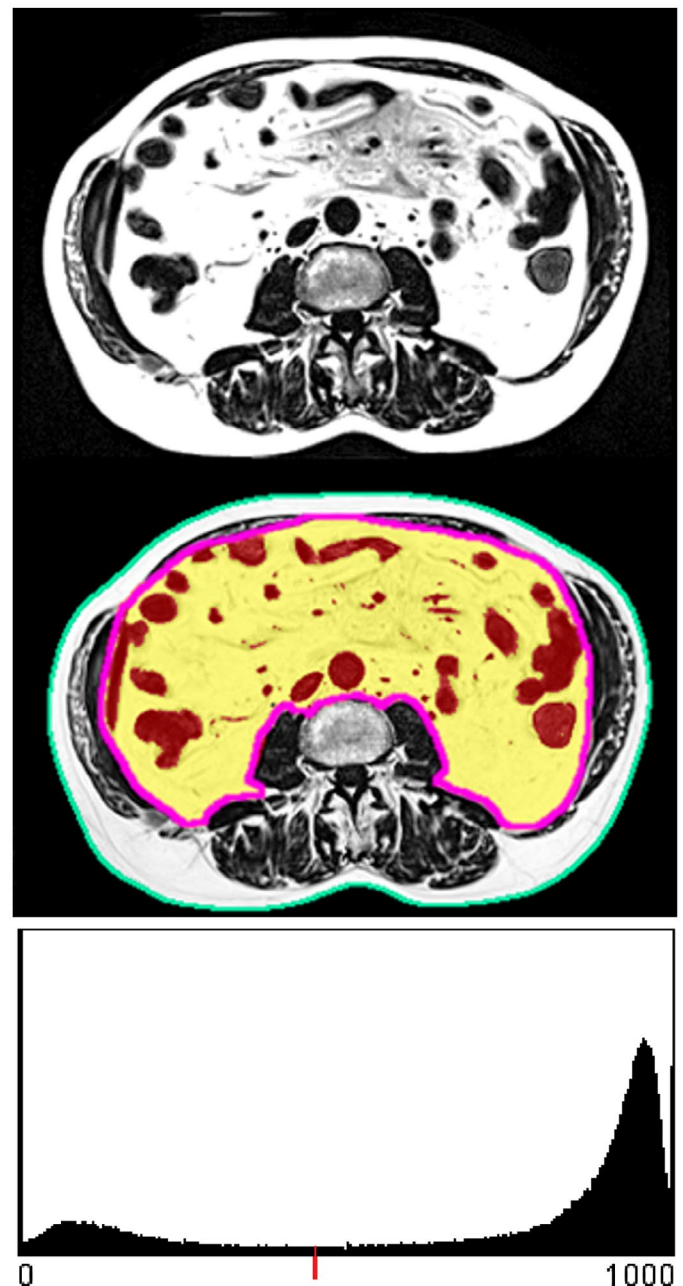
TABLE 1 Patient characteristics and BIA and MRI results for G1 (young healthy participants) and G2 (elderly participants) (mean ± SD) and *P* values of group differences (two-sample *t* test)

	G1	G2	*P*
Age, y	28 ± 4	76 ± 5	< 0.01
Weight, kg	76.5 ± 11.7	74.5 ± 7.8	0.45
Height, cm	181 ± 10	170 ± 5	< 0.01
BMI, kg/cm^2	23.1 ± 1.9	26.2 ± 2.4	< 0.01
BIA VFA, cm^2	38.6 ± 18	107.3 ± 29	< 0.01
MRI V$_{VAT}$, cm^3	283.4 ± 44.3	437.4 ± 89.0	< 0.01
MRI FF$_{VS}$, %	27.64 ± 8.03	59.78 ± 9.31	< 0.01
BIA BFM, kg	4.80 ± 2.22	11.85 ± 2.78	< 0.01
BIA BFP, %	12.8 ± 5.5	30.1 ± 4.5	< 0.01
MRI V$_{TAT}$, cm^3	610.5 ± 221.7	1,702.0 ± 352.4	< 0.01
MRI FF$_{TA}$, %	31.3 ± 8.6	58.9 ± 5.6	< 0.01

Weight, BMI, BFP, and VFA measured by segmental, multifrequency BIA. Fat fraction and volume of adipose tissue were measured by two-point Dixon MRI.
BFM, body fat mass; BFP, body fat percentage; BIA, bioelectrical impedance analysis; FF$_{TA}$, fat fraction of total abdominal volume of interest; FF$_{VS}$, fat fraction of visceral volume of interest; G1, group 1; G2, group 2; MRI, magnetic resonance imaging; V$_{TAT}$, volume of total adipose tissue; V$_{VAT}$, volume of visceral adipose tissue; VFA, visceral fat area.

Figure 1 Dixon MRI fat image of the abdomen (top). Segmentation results in the fat fraction map (middle): total abdominal (TA) volume of interest (VOI) is shown by the green contour; visceral (VS) VOI is shown by the magenta contour; the Otsu threshold separates VS adipose tissue (yellow overlay) from inner organs (dark red overlay). Histogram of the voxel values of the VS VOI (bottom): the red line marks the Otsu threshold, separating the two distinct peaks of high-fat and low-fat content.

MRI data acquisition and examination

All participants were scanned on a 3-T magnetic resonance system (MAGNETOM Skyra^fit; Siemens Healthcare GmbH, Erlangen, Germany).

Participants were imaged in a supine position with feet first toward the magnetic resonance system. A flexible 18-channel body radio-frequency surface coil wrapped around the abdominal area was used for signal reception and was activated together with a 32-channel radio-frequency spine array coil.

For fat imaging, a two-point Dixon gradient echo volumetric interpolated breath-hold examination technique was applied in breath-hold mode (axial plane matrix size: 320×240; resolution: 1.2×1.2 mm^2; repetition time (TR) $= 3.97$ milliseconds; echo time (TE) $1 = 1.29$ milliseconds; TE $2 = 2.52$ milliseconds; number of sections: 12; section thickness: 3.5 mm; distance factor: 20%; section gap: 0.7 mm; acquisition time $=$ 0:15 minutes). From the Dixon fat-only (I_F) and water-only (I_W) images, the FF images (I_{FF}) were calculated according to the following equation:

$$I_{FF} = \frac{I_F}{I_W + I_F} \times 1000.$$

The acquisition was centered on the disk between lumbar vertebrae L2 and L3. The total scan length of 5 cm approximately covered the region from mid-L2 to mid-L3.

Image processing started with the segmentation of the stack of fat images. The first section was omitted because of poor automatic bias correction. First, a fuzzy C-means clustering algorithm that separated voxels in the air from those inside the body was applied to the whole stack to determine the body surface and a total abdominal (TA) volume of interest (VOI). Then an operator previously trained by an expert radiologist manually segmented the visceral (VS) VOI section by section because, in our case, automatic methods (21,22) were not available. The abdominal and paraspinal muscles guided this segmentation. The VS VOI included internal organs but excluded the vertebral body and abdominal and paraspinal muscles (Figure 1).

An intensity threshold determined in the FF images by Otsu's (23) method was applied to all voxels of the VS VOI (Figure 1) to separate VAT from the internal organs. The same threshold was also used to separate adipose and nonadipose tissue compartments of the TA VOI. In analogy to VAT, the adipose tissue of the TA VOI will be abbreviated as total adipose tissue (TAT). The following measurements were made: First the volumes of VAT (V_{VAT}) and TAT (V_{TAT}), in centimeters cubed, were obtained as the number of voxels contained in VS and TA VOI, respectively, multiplied by the voxel volume. Second, the FF of VS VOI (FF$_{VS}$) and TA VOI (FF$_{TA}$) was measured as averages of the FF of all voxels of VS and TA VOI, respectively. Thus, the FF results contained contributions of the nonadipose tissue compartments of VS and TA VOI, respectively.

BIA measurements

Body height was determined by using calibrated devices. Body weight, overall body fat percentage (BFP), body fat mass (BFM) of the trunk in kilograms, and visceral fat area (VFA) in centimeters squared were estimated with segmental, multifrequency BIA (InBody770; InBody, Seoul, South Korea). Detailed information on how the parameters were derived was not provided by the manufacturer. The impedance of the trunk, arms, and legs was measured separately by using a tetrapolar eight-point tactile electrode system that applied six frequencies (1, 5, 50, 250, 500, and 1,000 kHz). To standardize the test procedure, participants were requested to refrain from severe physical activity 24 hours, and nutritional intake 3 hours, prior to the BIA assessment. MRI was performed immediately after the BIA investigation.

Statistical analysis

A simple linear regression analysis was used to predict MRI parameters from BIA measurements. Coefficients of determination (R^2), slopes, intercepts, and standard error of the estimates (SEE) were determined. In addition, Pearson correlation coefficients (r) were determined. Different intramodality comparisons were performed for each age group. The comparisons included adipose tissue volume and FF measurements from MRI and VFA and BFM estimates from BIA (Table 2). All statistical analyses were conducted in R version 3.3.2 (R Core Team, R Foundation for Statistical Computing, Vienna, Austria).

TABLE 2 Simple linear regression analyses for G1 (young healthy participants) and G2 (older participants)

Independent variable	Dependent variable	R^2, G1/G2	r, G1/G2	SEE, G1/G2, %	Slope, G1/G2	Intercept, G1/G2
BIA BFM	BIA VFA	0.97/0.95	0.99/0.98	7.7/5.2	0.12/0.09	0.22/1.82
MRI V$_{TAT}$	MRI V$_{VAT}$	0.69/0.65	0.87/0.89	20/12	1.93/0.95	141/808
MRI FF$_{TA}$	MRI FF$_{VS}$	0.75/0.78	0.84/0.81	14/4.5	0.94/0.54	5.44/26.8
BIA BFM	MRI V$_{TAT}$	0.44/0.54	0.68/0.74	27/14	68.1/94.2	284/598
BIA BFM	MRI FF$_{TA}$	0.56/0.31	0.76/0.57	18/8.0	2.95/1.16	17.1/45.3
BIA VFA	MRI V$_{TAT}$	0.38/0.48	0.64/0.70	28/15	7.67/8.41	314/794
BIA VFA	MRI FF$_{TA}$	0.53/0.25	0.74/0.52	19/8.3	0.34/0.10	18.0/48.3
BIA VFA	MRI V$_{VAT}$	0.20/0.22	0.49/0.49	35/28	2.5/5.0	145/401
BIA VFA	MRI FF$_{VS}$	0.44/0.13	0.68/0.39	22/15	0.30/0.12	16.2/46.5

Intramodality comparisons for BIA (BFM vs. VFA) and for MRI (V$_{VAT}$ vs. V$_{TAT}$ and FF$_{VS}$ vs. FF$_{TA}$). Intermodality comparisons shown in last six rows. Coefficient of determination (R^2) and Pearson correlation coefficient (r) as well as SEE as percentage of mean error are given. Last columns give slope and intercept of regression line.
BFM, body fat mass; BIA, bioelectrical impedance analysis; FF$_{TA}$, fat fraction of total abdominal volume of interest; FF$_{VS}$, fat fraction of visceral volume of interest; G1, group 1; G2, group 2; MRI, magnetic resonance imaging; SEE, standard error of estimates; V$_{TAT}$, volume of total adipose tissue; V$_{VAT}$, volume of visceral adipose tissue; VFA, visceral fat area.
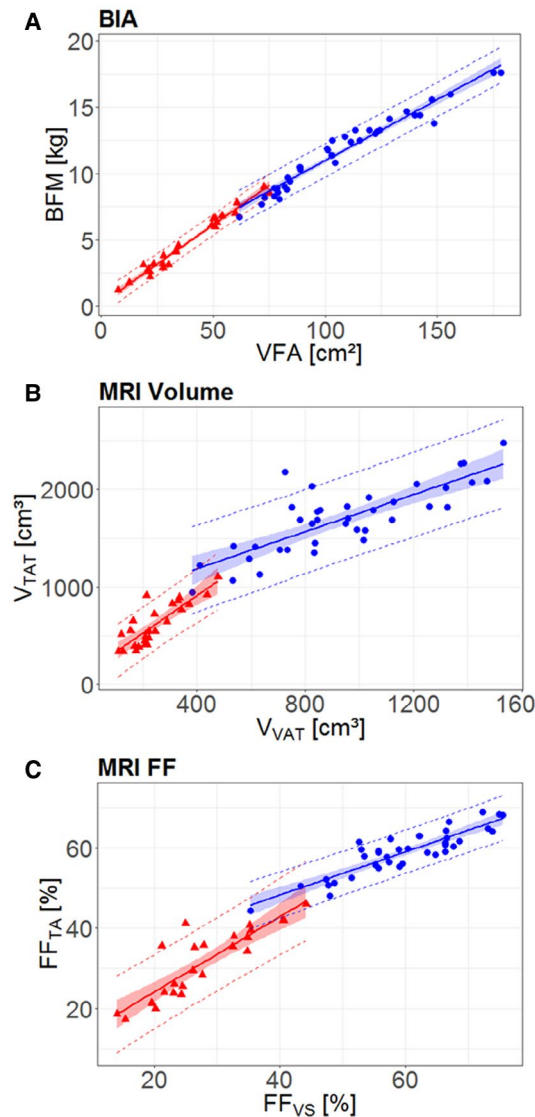
Figure 2 Intramodality comparisons between group 1 (red triangles: young healthy participants) and group 2 (blue dots: older participants). (**A**) Segmental, multifrequency bioelectrical impedance analysis (BIA): visceral fat area (VFA) in centimeters squared versus body fat mass (BFM) in kilograms of the trunk. (**B**) MRI volume: volume of total adipose tissue (V_{TAT}) versus visceral adipose tissue (V_{VAT}). (**C**) MRI fat fraction of total abdominal volume of interest (FF_{TA}) versus of visceral volume of interest (FF_{VS}). Solid lines indicate regression line with its 95% CI of the fit. Dashed lines show 95% prediction intervals of the linear model.

Results

Patient characteristics along with average MRI and BIA results are shown in Table 1. All 63 participants were examined successfully. Separate high-contrast and high-resolution fat and water images were obtained in all examinations (Figure 1). Fat-water swap artifacts were not observed. Table 2 shows intra- and intermodality linear regression results, which are graphically depicted in Figure 2 (intramodality comparisons) and Figures 3 and 4 (intermodality comparisons). Regressions were performed separately for G1 and G2, but results are shown for both groups in each graph.

For BIA, slopes and R^2 values were almost identical for both groups (Table 2, Figure 2). In contrast, slopes and R^2 values were smaller for all MRI comparisons. The slopes representing the rate of change with increasing VAT volume were significantly different between G1 and G2 ($P < 0.05$) (Figure 2).

Coefficients of determination between VFA and MRI VS measurements were poor. R^2 results were lower than 0.44 for both groups. SEE values were higher than those for corresponding regressions between VFA and MRI TA measurements (Table 2, Figure 3). In contrast, R^2 values between BFM and MRI TA measurements were similar to those between VFA and MRI TA measurements (Table 2). R^2 values between VFA and MRI V_{TAT} were higher, and SEE values were lower compared with those between VFA and MRI VS measurements (Table 2, Figure 4).

Discussion

In the current cross-sectional study, MRI results showed that the ratio of FF_{VS} to FF_{TA} was increased in older men compared with younger men. As expected, in the older population, FF was increased in both compartments (TA and VS), with a proportional higher increase of FF_{VS}. Interestingly, this differential effect could not be detected with the BIA technique, although in G2, an increase in FF of both compartments was also observed.

The large R^2 values, in combination with small SEE of the linear regressions of the VS and abdominal BIA estimates and almost identical slopes, indicated that these two parameters were rather identical. In contrast, the variation of the MRI VS measurements could be explained only in part by the variation of abdominal MRI measurements. SEE values for MRI were higher than those for BIA, and slopes differed by almost a factor of two. Moderate relationships between overall and VS fat levels were previously reported (24).

Apparently, the estimation of VFA with BIA is problematic. The regressions between BIA and MRI confirm this finding. BFM and VFA measured by BIA predicted MRI measurements equally well. For example, R^2 results between MRI FF_{TA} and BIA BFM were very similar to those between MRI FF_{TA} and BIA VFA. Moreover, the VS BIA estimates characterized the total VOI better than the VS VOI, although the opposite would be expected. These findings apply to both groups, but R^2 values of MRI FF versus BIA regressions were much lower in G2 compared with G1, whereas R^2 values of MRI fat volumes versus BIA regressions were similar for both groups. Thus, the BIA estimate of VS fat should be treated with caution; it may not carry additional information compared with the BIA BFM assessment of the TA compartment. The results of our study confirm similar findings after comparing BIA VFA assessments with fast-spin echo MRI scans (25).

In our analysis, we specifically did not exclude paraspinal and abdominal muscles from the total volume. Thus, FF_{TA} and V_{TAT} included contributions of intramuscular paraspinal and abdominal adipose tissue.

BIA and MRI variables were correlated; however, a comparison using Bland-Altman plots could not be performed because MRI FF was measured in percentages and fat volume in centimeters cubed and because BIA BFM was measured in kilograms and VS fat as the average area in centimeters squared. Moreover, MRI assessments were performed for the abdominal VOI, which was well defined by the section range selected for analysis. BIA signals were analyzed in the trunk, which covers more than the abdominal region. BIA BFM and MRI fat volume
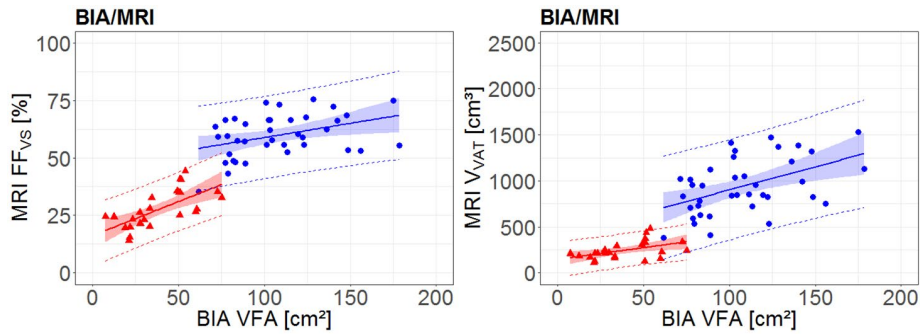
Figure 3 Intermodality comparison of bioelectrical impedance analysis (BIA) visceral fat area (VFA) with MRI fat fraction of the visceral volume of interest (FF$_{VS}$) (left) and MRI visceral adipose tissue volume (V$_{VAT}$) (right) between group 1 (red triangles: young healthy participants) and group 2 (blue dots: older participants). Solid lines represent regression line with its CI. Dashed lines represent prediction intervals for the linear model.
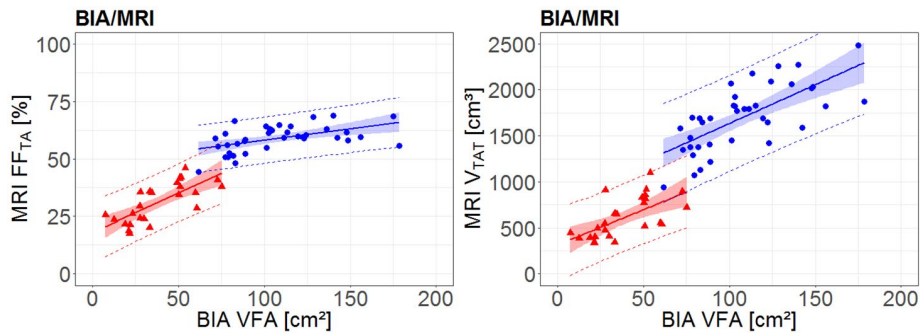

Figure 4 Intermodality comparison of bioelectrical impedance analysis (BIA) visceral fat area (VFA) with MRI fat fraction of the total abdominal volume of interest (FF$_{TA}$) (left) and MRI total abdominal adipose tissue volume (V$_{TAT}$) (right) between group 1 (red triangles: young healthy participants) and group 2 (blue dots: older participants). Solid lines represent regression line with its CI. Dashed lines represent prediction intervals for the linear model.

are related by the constant of physical density of fat, and indeed, correlations were moderate.

Another limitation of our study was the different anatomical coverage of the BIA and MRI measurements. Although specific information on the BIA coverage was not available from the manufacturer, from common BIA theory, it can be assumed that most of the trunk was included in the analysis. The MRI protocol covered a total length of only 5 cm of the lumbar region. This is another limitation of the study because with modern MRI sequences, the complete VS VOI can be measured in about 5 minutes.

There are probably methods to measure VAT more accurately, such as dual abdominal BIA. Unfortunately, validation and estimation of higher levels of VAT are still problematic with this method (26). Theoretically the different anatomical coverage of our BIA and MRI measurements could have contributed to the differences between BIA and MRI adiposity measurements. However, differences were larger in the VS than in the TA compartment. Also, it has been shown that the VS subregion used in this study was representative for the total VAT volume

(27-29). Even VAT obtained from a single MRI section located at the center of L3 correlated highly with whole abdominal VAT volume (30) ($r = 0.71$-0.94; $P < 0.05$). However, for longitudinal assessments, movement of the internal organs may have a large impact on the area of VAT assessed from a single section; thus, the acquisition of multiple sections is strongly advised (31).

The relatively large SEE of the linear regressions between MRI and BIA can be explained by several effects. One is the difference between abdominal and trunk regions assessed by the respective measurements; another, the limited precision of segmental, multifrequency BIA (32-34). In addition, body water, the only parameter measured and not estimated by BIA, is affected by the electrolyte balance, which depends on nutrition intake or exercise and differs between individuals and during the day (21,22,35-38). Therefore, BIA as well as multifrequency BIA results might be influenced by confounding factors, and these results should not be generalized to other BIA devices (38-40). To minimize these effects, participants were requested to refrain from severe physical activity 24 hours, and nutritional intake 3 hours, prior to the BIA assessment in the present study.

Most Dixon sequences were developed to quantify hepatic fat. Gold standard on Siemens scanners are multi-echo Dixon sequences; however in the thigh, and, in our experience, also in the abdomen, fat-water swap artifacts occur quite frequently, in particular in participants with low amounts of adipose tissue (41). Thus, we selected a simpler but more robust two-point Dixon sequence. In the thigh, the FF accuracy of this sequence was comparable with sequences using three or six echoes (16). Multiple-point Dixon sequences allow for more sophisticated postprocessing that addresses and corrects potential error sources in fat quantification. However, even multiple-point Dixon sequences do not measure glycogen, protein, minerals, etc.; thus, FF as measured by MRI Dixon sequences deviates from the true percentage of fat measured by chemical methods (42).

Two-point Dixon MRI delivers cross-sectional maps of the fat and water distribution with high spatial resolution. Because of high contrast, the adipose tissue of the VS compartment can easily be segmented by using a global threshold. Based on the histogram of the image, Otsu's (23) method automatically detects such a threshold. The histogram of Dixon FF images of the abdomen showed a distinct bimodal distribution between fat and lean tissue; thus the Otsu-based segmentation worked well. In contrast, T1-weighted images, as well as Dixon fat and water images, are affected by bias artifacts that, if uncorrected, spoil the bimodal distribution (Figure 1) (43,44). The bias artifacts are automatically eliminated in the FF images, a big advantage when using MRI Dixon sequences instead of T1-weighted MRI for determination of abdominal adipose tissue and, in particular, VAT. Although not the topic of this study, it should be noted that VAT is not pure fat. For the young men, the FF of the SAT VOI varied between 61% and 86%, and for the older men, the FF varied between 80% and 90%. The relevance of this observation for SAT area or volume measurements should be further investigated. This is another argument for preference of Dixon over T1-weighted measurements for the assessment of adipose tissue.

Conclusion

The FF of the TA and VS compartment was increased in older men compared with younger men. In the older patient cohort, there was a proportional higher increase of VS FF than in the younger group. VS BIA estimates agreed better with MRI measurements of the total abdomen than of the VS VOI, indicating that the BIA VS fat assessment cannot be used to differentiate adipose tissue differences between abdominopelvic VS and abdominal compartments in young and older participants. MRI Dixon sequences are the preferred method to differentiate abdominal and VS assessments of adipose tissue. In contrast to standard T1-weighted MRI, MRI Dixon sequences provide quantitative measurements from FF images that are not affected by bias artifacts. The exact calculation of body composition parameters by the BIA technique remains unknown, complicating the assessment of accuracy and the comparison across different body composition techniques.**O**

Acknowledgments

References

1. Hilton TN, Tuttle LJ, Bohnert KL, Mueller MJ, Sinacore DR. Excessive adipose tissue infiltration in skeletal muscle in individuals with obesity, diabetes mellitus, and peripheral neuropathy: association with performance and function. *Phys Ther* 2008;88:1336-1344.
2. Beasley LE, Koster A, Newman AB, et al. Inflammation and race and gender differences in computerized tomography-measured adipose depots. *Obesity (Silver Spring)* 2009;17:1062-1069.
3. Cruz-Jentoft AJ, Baeyens JP, Bauer JM, et al. Sarcopenia: European consensus on definition and diagnosis: report of the European Working Group on Sarcopenia in Older People. *Age Ageing* 2010;39:412-423.
4. Fischer-Posovszky P, Wabitsch M, Hochberg Z. Endocrinology of adipose tissue - an update. *Horm Metab Res* 2007;39:314-321.
5. Mazzali G, Di Francesco V, Zoico E, et al. Interrelations between fat distribution, muscle lipid content, adipocytokines, and insulin resistance: effect of moderate weight loss in older women. *Am J Clin Nutr* 2006;84:1193-1199.
6. Tuttle LJ, Sinacore DR, Mueller MJ. Intermuscular adipose tissue is muscle specific and associated with poor functional performance. *J Aging Res* 2012;2012:172957. doi:10.1155/2012/172957
7. Zoico E, Rossi A, Di Francesco V, et al. Adipose tissue infiltration in skeletal muscle of healthy elderly men: relationships with body composition, insulin resistance, and inflammation at the systemic and tissue level. *J Gerontol A Biol Sci Med Sci* 2010;65:295-299.
8. Shen W, Wang Z, Punyanita M, et al. Adipose tissue quantification by imaging methods: a proposed classification. *Obes Res* 2003;11:5-16.
9. Lakka HM, Laaksonen DE, Lakka TA, et al. The metabolic syndrome and total and cardiovascular disease mortality in middle-aged men. *JAMA* 2002;288: 2709-2716.
10. Rodriguez A, Catalán V, Gómez-Ambrosi J, Frühbeck G. Visceral and subcutaneous adiposity: are both potential therapeutic targets for tackling the metabolic syndrome? *Curr Pharm Des* 2007;13:2169-2175.
11. Jialal I, Devaraj S. Subcutaneous adipose tissue biology in metabolic syndrome. *Horm Mol Biol Clin Investig* 2018;33. doi:10.1515/hmbci-2017-0074
12. Sam S. Differential effect of subcutaneous abdominal and visceral adipose tissue on cardiometabolic risk. *Horm Mol Biol Clin Investig* 2018;33. doi:10.1515/hmbci-2018-0014
13. Lu HK, Chen YY, Yeh C, et al. Discrepancies between leg-to-leg bioelectrical Impedance analysis and computerized tomography in abdominal visceral fat measurement. *Sci Rep* 2017;7:9102. doi:10.1038/s41598-017-08991-y
14. Kullberg J, Johansson L, Ahlström H, et al. Automated assessment of whole-body adipose tissue depots from continuously moving bed MRI: a feasibility study. *J Magn Reson Imaging* 2009;30:185-193.
15. Ludwig UA, Klausmann F, Baumann S, et al. Whole-body MRI-based fat quantification: a comparison to air displacement plethysmography. *J Magn Reson Imaging* 2014;40:1437-1444.
16. Grimm A, Meyer H, Nickel MD, et al. Evaluation of 2-point, 3-point, and 6-point Dixon magnetic resonance imaging with flexible echo timing for muscle fat quantification. *Eur J Radiol* 2018;103:57-64.
17. Zhong X, Nickel MD, Kannengiesser SA, Dale BM, Kiefer B, Bashir MR. Liver fat quantification using a multi-step adaptive fitting approach with multi-echo GRE imaging. *Magn Reson Med* 2014;72:1353-1365.
18. Nickel MD, Kannengiesser SAR, Kiefer B. Time-domain calibration of fat signal dephasing from multi-echo STEAM spectroscopy for multi-gradient-echo imaging based fat quantification. In: Proceedings of the 23rd Annual Meeting of the International Society for Magnetic Resonance in Medicine; May 30-31, 2015; Toronto, Canada. Abstract 3658.
19. Ling CH, de Craen AJ, Slagboom PE, et al. Accuracy of direct segmental multi-frequency bioimpedance analysis in the assessment of total body and segmental body composition in middle-aged adult population. *Clin Nutr* 2011;30:610-615.
20. Kemmler W, Weissenfels A, Teschler M, et al. Whole-body electromyostimulation and protein supplementation favorably affect sarcopenic obesity in community-dwelling older men at risk: the randomized controlled FranSO study. *Clin Interv Aging* 2017; 12:1503-1513.
21. Langner T, Hedström A, Morwald K, et al. Fully convolutional networks for automated segmentation of abdominal adipose tissue depots in multicenter water-fat MRI. *Magn Reson Med* 2019;81:2736-2745.

22. Shen J, Baum T, Cordes C, et al. Automatic segmentation of abdominal organs and adipose tissue compartments in water-fat MRI: application to weight-loss in obesity. *Eur J Radiol* 2016;85:1613-1621.

23. Otsu N. A threshold selection method from gray-level histograms. *IEEE Trans Syst Man Cybern* 1979;9:62-66.

24. Enzi G, Gasparo M, Biondetti PR, Fiore D, Semisa M, Zurlo F. Subcutaneous and visceral fat distribution according to sex, age, and overweight, evaluated by computed tomography. *Am J Clin Nutr* 1986;44:739-746.

25. Browning LM, Mugridge O, Chatfield MD, et al. Validity of a new abdominal bioelectrical impedance device to measure abdominal and visceral fat: comparison with MRI. *Obesity (Silver Spring)* 2010;18:2385-2391.

26. Park KS, Lee DH, Lee J, et al. Comparison between two methods of bioelectrical impedance analyses for accuracy in measuring abdominal visceral fat area. *J Diabetes Complications* 2016;30:343-349.

27. Schaudinn A, Linder N, Garnov N, et al. Predictive accuracy of single- and multi-slice MRI for the estimation of total visceral adipose tissue in overweight to severely obese patients. *NMR Biomed* 2015;28:583-590.

28. Maislin G, Ahmed MM, Gooneratne N, et al. Single slice vs. volumetric MR assessment of visceral adipose tissue: reliability and validity among the overweight and obese. *Obesity (Silver Spring)* 2012;20:2124-2132.

29. Demerath EW, Shen W, Lee M, et al. Approximation of total visceral adipose tissue with a single magnetic resonance image. *Am J Clin Nutr* 2007;85:362-368.

30. Schweitzer L, Geisler C, Pourhassan M, et al. Estimation of skeletal muscle mass and visceral adipose tissue volume by a single magnetic resonance imaging slice in healthy elderly adults. *J Nutr* 2016;146:2143-2148.

31. Shen W, Chen J, Gantz M, Velasquez G, Punyanitya M, Heymsfield SB. A single MRI slice does not accurately predict visceral and subcutaneous adipose tissue changes during weight loss. *Obesity (Silver Spring)* 2012;20:2458-2463.

32. Sun G, French CR, Martin GR, et al. Comparison of multifrequency bioelectrical impedance analysis with dual-energy X-ray absorptiometry for assessment of percentage body fat in a large, healthy population. *Am J Clin Nutr* 2005;81:74-78.

33. Dehghan M, Merchant AT. Is bioelectrical impedance accurate for use in large epidemiological studies? *Nutr J* 2008;7:26. doi:10.1186/1475-2891-7-26

34. Buckinx F, Reginster JY, Dardenne N, et al. Concordance between muscle mass assessed by bioelectrical impedance analysis and by dual energy X-ray absorptiometry: a cross-sectional study. *BMC Musculoskelet Disord* 2015;16:60. doi:10.1186/s12891-015-0510-9

35. Androutsos O, Gerasimidis K, Karanikolou A, Reilly JJ, Edwards CA. Impact of eating and drinking on body composition measurements by bioelectrical impedance. *J Hum Nutr Diet* 2015;28:165-171.

36. Slinde F, Rossander-Hulthén L. Bioelectrical impedance: effect of 3 identical meals on diurnal impedance variation and calculation of body composition. *Am J Clin Nutr* 2001;74:474-478.

37. Thompson DL, Thompson WR, Prestridge TJ, et al. Effects of hydration and dehydration on body composition analysis: a comparative study of bioelectric impedance analysis and hydrodensitometry. *J Sports Med Phys Fitness* 1991;31:565-570.

38. Gualdi-Russo E, Toselli S. Influence of various factors on the measurement of multifrequency bioimpedance. *Homo* 2002;53:1-16.

39. Kushner RF, Gudivaka R, Schoeller DA. Clinical characteristics influencing bioelectrical impedance analysis measurements. *Am J Clin Nutr* 1996;64:423S-427S.

40. Kyle UG, Bosaeus I, De Lorenzo AD, et al. Bioelectrical impedance analysis, part II: utilization in clinical practice. *Clin Nutr* 2004;23:1430-1453.

41. Grimm A, Meyer H, Nickel MD, et al. A comparison between 6-point Dixon MRI and MR spectroscopy to quantify muscle fat in the thigh of subjects with sarcopenia. *J Frailty Aging* 2019;8:21-26.

42. Hines CD, Yu H, Shimakawa A, McKenzie CA, Brittain JH, Reeder SB. T1 independent, T2* corrected MRI with accurate spectral modeling for quantification of fat: validation in a fat-water-SPIO phantom. *J Magn Reson Imaging* 2009;30:1215-1222.

43. Reeder SB, Sirlin CB. Quantification of liver fat with magnetic resonance imaging. *Magn Reson Imaging Clin N Am* 2010;18:337-357, ix.

44. Fallah F, Machann J, Martirosian P, Bamberg F, Schick F, Yang B. Comparison of T1-weighted 2D TSE, 3D SPGR, and two-point 3D Dixon MRI for automated segmentation of visceral adipose tissue at 3 Tesla. *MAGMA* 2017;30:139-151.